OPTO-ELECTRONICS REVIEW **14**(1), 71–77

Interfaces as design tools for short-period InAs/GaSb type-II superlattices for mid-infrared detectors

F. SZMULOWICZ*, H.J. HAUGAN[1,2], G.J. BROWN[1,3], K. MAHALINGAM, B. ULLRICH[1,3], S.R. MUNSHI[4], and L. GRAZULIS[1,2]

[1]Air Force Research Laboratory, Materials & Manufacturing Directorate, Wright-Patterson AFB, OH, 45433-7707 USA
[2]University of Dayton Research Institute, 300 College Park, Dayton, OH, 45469-0178 USA
[3]Universal Technology Corporation, Dayton, OH, 45432-2600 USA
[4]Centers for Materials and Photochemical Sciences, Department of Physics and Astronomy, Bowling Green State University, Bowling Green, OH, 43403-0224 USA

The effect of interface anisotropy on the electronic structure of InAs/GaSb type-II superlattices is exploited in the design of thin-layer superlattices for mid-IR detection threshold. The design is based on a theoretical envelope function model that incorporates the change of anion and cation species across InAs/GaSb interfaces, in particular, across the preferred InSb interface. The model predicts that a given threshold can be reached for a range of superlattice periods with InAs and GaSb layers as thin as a few monolayers. Although the oscillator strengths are predicted to be larger for thinner period superlattices, the absorption coefficients are comparable because of the compensating effect of larger band widths. However, larger intervalence band separations for thinner-period samples should lead to longer minority electron Auger lifetimes and higher operating temperatures in p-type SLs. In addition, the hole masses for thinner-period samples are on the order the free-electron mass rather than being effectively infinite for the wider period samples. Therefore, holes should also contribute to photoresponse. A number of superlattices with periods ranging from 50.6 to 21.2 Å for the 4 μm detection threshold were grown by molecular beam epitaxy based on the model design. Low temperature photoluminescence and photoresponse spectra confirmed that the superlattice band gaps remained constant at 330 meV although the period changed by the factor of 2.5. Overall, the present study points to the importance of interfaces as a tool in the design and growth of thin superlattices for mid-IR detectors for room temperature operation.

Keywords: superlattice, infrared detector, InAs/GaSb, interface, envelope function.

1. Introduction

Beginning with their proposal by Smith and Mailhiot [1,2] InAs/InGaSb superlattices (SLs) have been exploited as detectors and lasers operating in the short to very long infrared (IR) wavelength regions [3–5]. There is particular interest in thermal imaging in the mid-IR detection range (3 to 5 μm) using binary/binary InAs/GaSb uncooled IR detectors [6,7] for room temperature operation [8,9]. These systems feature the type-II band alignment wherein the valence band of GaSb is some 150 meV above the conduction band of InAs [1,2]. By proper choice of layer widths, it is possible to tune not only the SL band gaps but also other key features of the band structure in order to optimize optical absorption or reduce Auger recombination and tunneling currents [8,9]. In this paper, we show that the interface is another design parameter that can be profitably exploited to band gap engineer mid-IR, thin-layer SLs. Our model employs the 8×8 envelope function approximation (EFA) that has been modified to include interface effects [10].

An ideal interface in the NCA InAs/GaSb system contains either InSb or GaAs bonds, compounds that are not present in the SL proper. In III–V heterojunctions with noncommon anions or cations grown in the [001] direction, adjacent rows of atoms are at right angles to each other, so that the true interface (IF) symmetry is C_{2v} rather than C_{2d} [11]. The lowering of the symmetry causes heavy hole (HH) and light hole (LH) bands to interact (repel), so that the electronic structure of InAs/GaSb SLs becomes a strong function of interface type as well as layer width [10]. The EFA has successfully modelled IF effects using short-range delta function potentials centered at the Ifs [12–16]. The EFA has the physical appeal of being more directly connected to the quantities being modelled and for being more physically transparent [17–18]. The standard

*e-mail: Frank.Szmulowicz@wpafb.af.mil
The paper presented there appears in *Infrared Photoelectronics*, edited by Antoni Rogalski, Eustace L. Dereniak, Fiodor F. Sizov, Proc. SPIE Vol. 5957, 595708 (2005).

EFA extended to model IF anisotropy in NCA SLs has been able to account for their giant absorption anisotropy [11,19–22] and spin-relaxation behaviour.

The physical picture underlying the present interface design is as follows [10]. With decreasing GaSb width, the bottom of the conduction band and the top of the (HH) valence band decrease in energy [10,23,24]. The lowering of the top of the valence band is the consequence of the size quantization of HH that are localized in GaSb. The conduction electrons are less affected by size quantization since they are delocalized over the entire SL. As a result, as the GaSb width decreases, the width of the conduction band broadens while its centroid remains constant so that the bottom of the conduction band decreases in energy as well. However, the rate at which these band edges decrease in energy depends on their interactions with other bands. Without IF interactions, both band edges move at the same rate so that the band gap remains constant. With IF interactions included, the top of the valence band decreases at a slower rate so that the overall band gap decreases [10]. In order to maintain the same gap, the InAs width can be made smaller in order to increase the size quantization of electrons in the InAs layer (i.e., raise the conduction band centroid). Therefore, it should be possible to design SLs for a given threshold with thin GaSb and InAs layers. It is the purpose of this work to demonstrate and validate these designs and to explore their advantages.

This paper is organized as follows. Section II describes the EFA model modified to account for NCA IF effects. The model is then used to design mid-IR SLs for the 4 μm detection range (310 meV). Section III describes the growth of the proposed SL structures by molecular beam epitaxy (MBE), their characterization by x-ray diffraction, atomic force microscopy, photoluminescence, and photoresponse measurements, and the comparison of model predictions with experimental data. Conclusions are presented last.

2. Theory

2.1. Interface effects in the EFA theory

InAs/GaSb SLs are non-common-atom (NCA) systems in which the identity of both anions and cations changes across each interface [11]. Therefore, two types of interfaces are possible – GaAs-like and InSb-like – with the latter being preferred for being smoother and leading to better carrier mobilities and lifetimes. As a result, for (001)-grown SLs, the [110] and [–110] directions are nonequivalent, which reduces the symmetry of an interface from D_{2d} to C_{2v} [11,19–22] In C_{2v} symmetry, there is no symmetry operation that can turn an atom on one side of the interface into an atom on the other side. This reduction of symmetry introduces interactions not present in common-atom systems; in particular, the heretofore noninteracting HH and LH valence bands become coupled and repel one another.

The first experimental manifestations of interface anisotropy was the observation of the giant in-plane optical anisotropy of NCA group-III SLs. Krebs and Voisin [11] explained this effect by the reduction of the assumed D_{2d} symmetry to the C_{2v} symmetry. They modelled the effect in the EFA via a short-range (delta) potential at SL IFs [12,25], whose short range was subsequently proved rigorously by Foreman [26] and Takhtamirov and Volkov [25]. The same theory was also used recently to calculate the hole-spin relaxation times and absorption spectra in InAs/GaSb SLs [27–30].

A closely related theory of Ivchenko-Kaminski-Rössler [12] is based on the theory of invariants in which group theory is used to posit the form of the additional interaction due to IF anisotropy. The strength of the interaction is an experimental fitting parameter, one each for the two interface types. The additional term in the Hamiltonian has the form

$$V = H_{XY}\, a_0 \delta(z) \Theta, \tag{1}$$

where H_{XY} is the strength of the IF potential, a_0 is the lattice constant, $\delta(z)$ is the Dirac delta function, and Θ is an 8×8 matrix with nonzero entries for the bands that are coupled by the interaction. For an IF with the C_{2v} symmetry, Θ has nonzero terms for the interaction of the HH and LH bands as well as of the HH and spin-orbit (SO) bands. Additional refinements introduced by Takhtamirov and Volkov [25] extend the applicability of the theory to graded interfaces.

When the IF interaction is used to set up the boundary conditions, the symmetry lowering introduced by NCA IFs contributes to the mismatch of the derivative of the envelope function at the IF in addition to that already present in the EFA due to the effective mass discontinuity at the IFs. The size of the mismatch depends on the strength of the interaction H_{XY} and the amplitude of the envelope functions at the IFs. In the present calculation, the effect of the interface potential is included exactly in the boundary conditions, that is, nonperturbatively [10].

2.2. Model examples

The effect of the anisotropic IF interaction can be better appreciated by considering a few limiting cases [10]. Consider a hypothetical type-II alignment of two materials A and B in which parabolic HH and LH bands are coupled by the anisotropic interface potential only. The EFA Hamiltonian for such a system is

$$\begin{pmatrix} -\dfrac{\hbar^2}{2m_H}\dfrac{d^2}{dz^2} & iT\delta(z) \\ -iT\delta(z) & -\dfrac{\hbar^2}{2m_L}\dfrac{d^2}{dz^2} \end{pmatrix} \begin{pmatrix} F_H(z) \\ F_L(z) \end{pmatrix} = E \begin{pmatrix} F_H(z) \\ F_L(z) \end{pmatrix}, \tag{2}$$

where the strength of the interaction $T = H_{XY}\, a_0 / \sqrt{3}$, $m_{H,L}$ are the HH and LH masses, and $F_{H,L}$ are the corre-

sponding envelope functions. This Hamiltonian has a bound state solution with the energy [10]

$$E = -\frac{T^2}{2\hbar^2}\sqrt{m_L m_H}, \tag{3}$$

a number on the order of several meV for the material parameters of GaSb and InAs and is independent of the sign of T, but clearly depends on $HH - LH$ coupling.

Next consider a quantum well in which size quantization competes with IF localization. The situation can be modelled with the simple Hamiltonian [10]

$$\begin{pmatrix} -\frac{\hbar^2}{2m_H}\frac{d^2}{dz^2} + V(z) & iT[\delta(z-b) - \delta(z+b)] \\ -iT[\delta(z-b) - \delta(z+b)] & -\frac{\hbar^2}{2m_L}\frac{d^2}{dz^2} + V(z) \end{pmatrix} \times \begin{pmatrix} F_H \\ F_L \end{pmatrix} = E\begin{pmatrix} F_H \\ F_L \end{pmatrix} \tag{4}$$

where

$$V(z) = \begin{cases} 0 & |z| \le b \\ V_0 & |z| > b \end{cases}. \tag{5}$$

V_0 denotes the depth of the potential and $2b$ is the width of the well. Solving the EFA Hamiltonian for this case gives two separate conditions:

- for the coupled even parity HH-odd parity LH manifolds (for example, HH1 and LH2 states), for which

$$\begin{aligned} &(k_L \cot k_L b + \kappa_L)(k_H \tan k_H b - \kappa_H) \\ &+ (2T/\hbar^2)^2 (m_H m_L) = 0 \end{aligned}, \tag{6}$$

  where

$$k_{H,L} = \sqrt{2m_{H,L}\, E/\hbar^2}$$

  and

$$\kappa_{H,L} = \sqrt{2m_{H,L}\,(V_0 - E)/\hbar^2}.$$

  Absent the coupling, the two parentheses separately give conditions for the even parity HH and odd parity LH states, respectively;

- for the coupled even parity LH – odd parity HH manifolds (for example, LH2 and HH1), one finds

$$\begin{aligned} &(\kappa_H + k_H \cot k_H b)(\kappa_L - k_L \tan k_L b) \\ &-(2T/\hbar^2)(m_H m_L) = 0 \end{aligned}. \tag{7}$$

  Absent the coupling, the two parentheses give conditions for odd parity HH and even parity LH states, respectively.

Figure 1 demonstrates the size of the effect. using realistic parameters for a hole in the GaSb layer surrounded on both sides by InAs, well depth V_0 = 560 meV, m_H = 0.267 m_0, m_L = 0.050 m_0, and T = (625 meVÅ)t, where t is dimensionless. As a function of interface coupling strength t, Fig. 1 display two ladders (HH and LH) of size quantized states. In the limit of large t, the lowest HH and LH states are bound at interfaces. State hybridization and level repulsion are evident. Similar effects are operative in SLs [10].

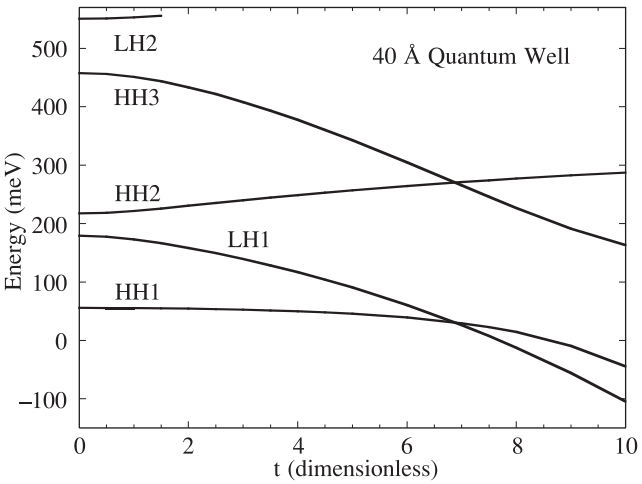

Fig. 1. The energy levels for a 40 Å quantum well with symmetric interfaces as a function of the dimensionless interface coupling constant t[T = (625 meVÅ)t]. The well depth V_0 = 560 meV, m_H = 0.267 m_0, and m_L = 0.050 m_0 is appropriate for a GaSb well inside InAs. At t = 0, the eigenstates can be labelled as heavy (HH) or light (LH). LH1 and HH1 become bound for larger couplings.

2.3. Tests of the model on real samples

The present theory was tested on several sets of samples grown in-house and elsewhere. The first in-house set consisted of four SLs with GaSb widths from 18 to 27 Å and a constant InAs width of 20.5 Å, all with InSb IFs [10,31,32]. The value of H_{XY} = 580 meV, or t = 5.66, was found by fitting the gap of one of the samples and then was used throughout, including the present paper [10]. The second in-house set consisted of five SLs with InAs widths from 16 to 23.5 Å and a constant GaSb width of 24 Å, all with InSb IFs. Without additional fitting parameters, the calculations were repeated for several long-wavelength samples from Northwestern University: the 19 μm sample of Wei *et al.* [33] and the 32 μm sample of Wei *et al.* [34] also with InSb IFs. Lastly, two sets of samples with mixed interfaces from Ongstad *et al.* [23] and Kaspi *et al.* [24] were used with H_{XY} = 580 meV for InSb-like IFs and a small number for GaAs-like IFs that was found by fitting the gap of their 6 ML/6 ML sample. The measured band gaps for all these samples agreed very well with the results of the calculations with the effects of IFs included. Without these effects, the calculated results disagreed with data both quantitatively and qualitatively [10].

2.4. Design of thin-layer mid-IR SL structures

In SL design, IF effects present both a problem and an opportunity. The problem is that real interfaces can be interdiffused, alloyed, atomically segregated, graded, and rough to a degree that can be difficult to quantify or reproduce in subsequent growths. As a result, such IFs can be hard to model. However, IF effects represent another degree of freedom in SL design. For example, the different

lattice constants of the InSb and GaAs IF bonds have long been exploited to design and grow strain-free InAs/GaSb SLs [35]. Moreover, InSb-like IFs have been preferred for yielding smoother interfaces with better carrier mobilities.

In this paper, we use IF effects to control the band gap and other properties of the resulting SL. As an example, Fig. 2 shows the band structure calculated with our modified 8×8 EFA model for one of the samples in the study, a 23.9 Å GaSb/20.4 Å InAs SL with both InSb IFs. The material input parameters for the present calculation are the same as in our previous study (H_{XY} = 580 meV or t = 5.66) [10]. The zero of energy is at the bottom of the conduction band of unstrained InAs. The bands are labeled according to their dominant character so that the top of the valence band is predominantly HH while the lower bands are of a mixed HH/LH character. The conduction band is predominantly C-like, but an admixture of LH and SO components from the coupling terms in the $\boldsymbol{k} \bullet \boldsymbol{p}$ Hamiltonian leads to the observed spin-splitting away from the zone centre; otherwise, the C band is not directly coupled to other bands by the IF terms.

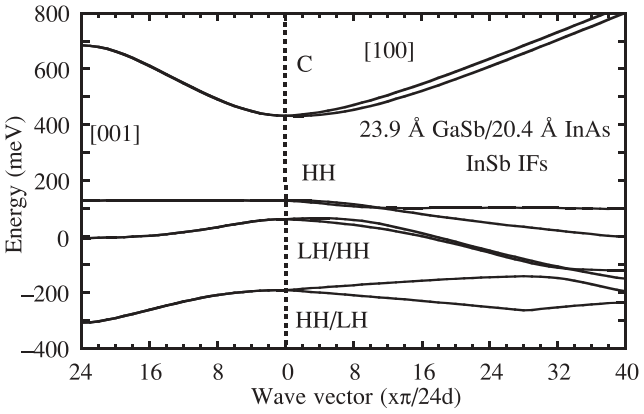

Fig. 2. The calculated band structure of a thicker-period, 23.9 Å GaSb/20.4 Å InAs SL with two InSb IFs along the growth [001] and in-plane [100] directions The Brillouin zone in the growth direction has the width $2\pi/d$, where d is the lattice period. The valance bands have a mixed HH/LH character.

The band gap is 304.2 meV but, without IF effects, the band gap would have been 391.5 meV. The proximate cause of the smaller band gap is the level repulsion between the HH-like top of the valence band and the LH-like bands below it. Along the [001]-axis, the bands are doubly degenerate since the SL as a whole has the D_{2d} symmetry because the two IFs are the same. The lowered symmetry of the SL manifests itself in the spin-split bands along the [100]-axis and a number of avoided band crossings. The electron effective mass is $m_{\|}^{C} = 0.0316$ in the growth direction. The HH band is about 1 meV wide in the growth direction so that $m_{\|}^{HH}$ is effectively infinite.

For comparison, the band structure of a thinner period SL (9.9 Å GaSb/11.4 Å InAs with 2 InSb-like IFs) in Fig. 3

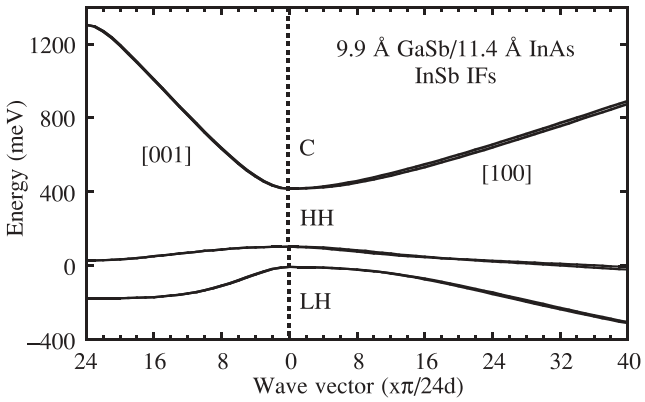

Fig. 3. Same as Fig. 2 for a thinner-period SL – 9.9 Å GaSb/11.4 Å InAs with two InSb-like IFs. The C band width in the growth direction is considerably broader than for the wider-period SL, Fig. 2. Note that the vertical scale is greater than in Fig. 2 and that the horizontal scale is inversely proportional to d.

differs from that in Fig. 2 in several respects. Most importantly, as the result thinner GaSb layer, the electron wave function overlap between adjacent InAs layers is stronger so that the conduction band width in the growth direction increases from 251 meV to 888 meV. The electron effective mass is $m_{\|}^{C} = 0.0304$ in the growth direction. The HH band width increases from 1 to 75 meV so that $m_{\|}^{HH} = 0.678$ is finite and on the order of the free electron mass, which should lead to better transport by holes, thus better gain. On the other hand, the joint density of states is smaller, which will counteract the increase in oscillator strength owing to greater wave function overlap (see the discussion following Fig. 4). The band gap is 313.8 meV but, without IF effects, it would have been 514.6 meV.

The spin-splitting in Fig. 3 is smaller than in Fig. 2 for the wider period SL as the result of the delocalization of hole wave functions over the entire SL. Lastly, in Figs. 2 and 3, the top two valence bands are separated by 65 and 109 meV, respectively. Therefore, for thinner-period SLs, as the result of size quantization, the lower valence bands are further removed from the top of the valence band. This should act to discourage the Auger recombination of minority electrons in p-type SLs and lead to higher detector operating temperatures [27,30].

Our strategy in the design of thin-layer mid-IR samples is as follows. An initial design with thick layers is first identified for some combination of InAs and GaSb layer widths (for example, Fig. 2). Starting with this initial design, the GaSb width is decreased by one monolayer, which leads to a smaller band gap since the conduction band decreases in energy faster than the top of the valence band. In order to keep the band gap constant, the InAs layer is made narrower to exploit electron size-quantization in the InAs layer to push the conduction band higher. With a proper choice of layer widths, the band gap can be kept constant as the SL period is shortened.

Using this process, several SL structures with InSb-like IFs were designed for the 4-μm detection threshold, Table 1.

Table 1. Design parameters and calculated properties of several InAs/GaSb SLs with InSb interfaces for the 4 micron detection threshold. The GaSb and InAs layer widths already include the width of one InSb-like interface each. HH1 and C1 refer to the top and bottom of the valence and conduction bands, respectively. A few lower-lying valence bands of mixed LH/HH character are also listed. The zero of energy is at the bottom of the conduction band of unstrained InAs, and the unstrained GaSb/InAs valence-conduction band offset is 150 meV.

GaSb width (Å)	InAs width (Å)	Period (Å)	LH/HH (meV)	HH1 (meV)	C1 (meV)	Band gap (meV)	Oscillator strength (Rydbergs)
28.4	21.9	50.3	77.22 –130.46	131.59	438.14	306.55	0.457
23.9	20.4	44.3	63.04 –190.70	128.69	432.90	304.21	0.502
15.9	15.9	31.8	30.10	119.83	429.09	309.2	0.507
11.4	12.9	24.3	2.11	107.63	415.65	308.2	0.690
9.9	11.4	21.3	–6.84	102.81	416.58	313.77	0.723
6.9	9.9	16.8	–46.21	71.24	371.47	300.23	0.761

The table includes the positions of the HH1, C1, and LH-like levels at the zone centre as well as the gap and oscillator strengths. A separate examination of the wave function content reveals that for the top two samples, the first LH-like level below HH1 is evenly HH/LH mixed. For the other, thinner, samples, that level is predominantly LH-like. For narrower SLs, the third valence band moves down considerably in energy. The most striking aspect of the table is the prediction that the gap can remain constant at 4 μm (300 meV) with decreasing SL period. For thinner SLs, the wave functions become delocalized over the entire SL so that the HH1-C1 wave function overlap increases (spatially indirect intersubband transition) as does the corresponding oscillator strength (the last column of Table 1).

Using the design parameters from Table 1, the full band structure and oscillator strengths were calculated and then used to obtain the linear absorption coefficient, Fig. 4. The absorption thresholds are at the band gap energies listed in Table 1. Additional thresholds can be seen in the curves for transitions from the lower valence band states to the conduction band. The absorption coefficients within 200 meV of the threshold energy are nearly the same for all the designs so that the increased oscillator strengths at threshold for narrow periods, Table 1, are compensated by correspondingly lower joint densities of states due to the broadening of the valence band. The proposed SL structures in Table 1 were grown and characterized as described next.

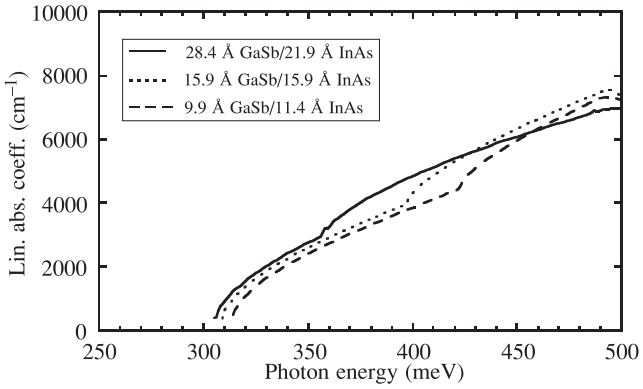

Fig. 4. The calculated linear absorption coefficient for a few representative samples from Table 1. The absorption threshold is at the onset of transitions from the HH-like top of the valence band. The second threshold at higher energies is the onset of transitions from the mixed HH/LH valence band.

3. Growth, measurement, and comparison with model

3.1. Experiments

The InAs/GaSb SL structures were grown by Gen-II molecular beam epitaxy (MBE) system on epi-ready (100) p-type GaSb wafers using elemental metals for Ga and In and valved cracker cells for Sb and As. The SL layers were grown at the substrate temperature of 390 ±10°C with the V/III beam flux ratio of 3 for growing InAs and 2.5 for growing GaSb [36]. Since most of the proposed designs are relatively thin, the control of individual layer thicknesses and interfaces in the formation of the intended structure is critical for the mid-IR design study. In the present work, the layer thicknesses of GaSb, InAs and InSb were controlled by using the slow growth rates of 0.96, 0.27 and 0.33 Å/s, respectively. By this method, the intended periods could be attained accurately to within the experimental error of 0.3%. Although we cannot assess the degree of interface intermixing, we kept the interface conditions constant during all the growths in order to form consistent InSb-like IFs between the layers. With InSb-like IF bonds, the overall SL strain was reduced, although the degree of strain varies with design. Grown samples were characterized by high-resolution x-ray rocking curve (HRXRD) measurements to determine the SL periods and by high resolution transmission electron microscopy (HRTEM) to examine the quality of the grown structures. The band gaps of the grown SLs were measured with a Fourier transform infrared (FTIR) spectrometer and by low temperature photoluminescence.

3.2. Results

In order to compare the parameters of the grown and intended SL structures, the SL periods were determined by HRXRD measurements. For the thirteen samples used in this study, the measured periods were within 0.3% of the intended periods. While SL periods can be accurately determined with XRD, the individual layer thicknesses are less well known; however, on the basis of growth calibrations and HRTEM measurements, they are expected to be close to the intended values.

Figure 5 is a high-resolution transmission electron microscope (HRTEM) image of the SL structure showing the individual layers of InAs and GaSb, with well-defined IFs. The position of the IFs is identified by observing the distinct shift in the bright and dark dots between the individual layers. Detailed examination of several such regions revealed that the transition from one layer to another occurred within 1–2 ML, thereby indicating both the high quality and the uniformity of the IFs within the SL. This further enabled an accurate measurement of the individual layer-thicknesses, which was performed by counting the number of monolayers between each IF.

The optical band gaps of the grown SL structures were obtained from the peak positions in 5K PL and the long-wavelength thresholds in FTIR photoresponse spectra. The experimental data is shown together with model calculations in Fig. 6.

3.3. Comparison to measurement

The model predictions of the EFA theory are compared to the measured PL peak energies and the long-wavelength thresholds in FTIR photoresponse in Fig. 6, where for convenience the data are plotted versus SL period. The PL peaks are clustered within a narrow band between 340 and 325 meV as the period changes from 50.6 to 21.2 Å. The predicted gaps cluster around 310 meV. The 15 to 30 meV difference is smaller than the expected experimental errors

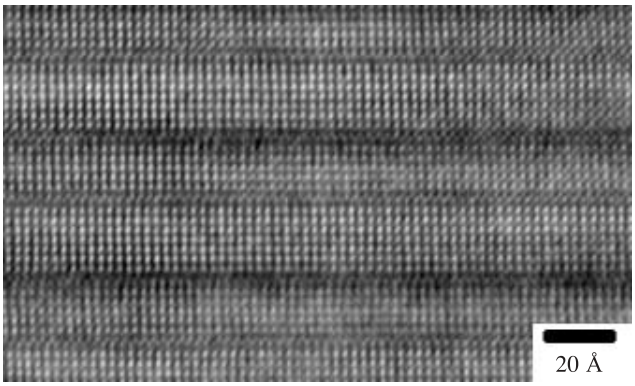

Fig. 5. A [010] cross-sectional HRTEM image of an InAs-GaSb superlattice structure showing smooth and abrupt interfaces between the individual layers. The intended individual layer thicknesses for this structure were 20.5 Å for InAs, and 24 Å for GaSb.

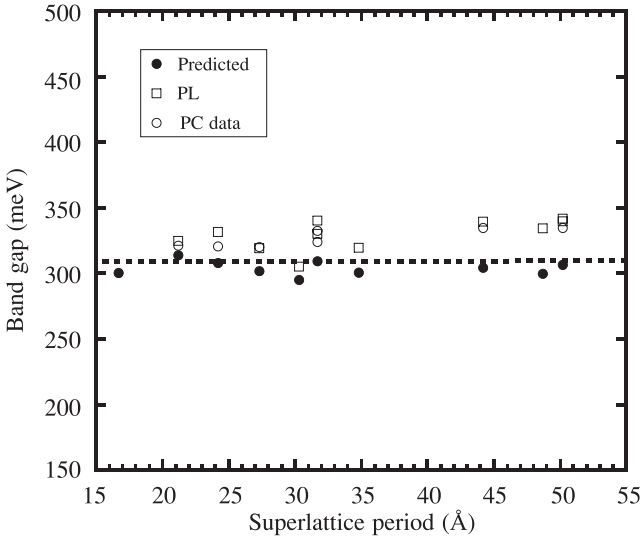

Fig. 6. Comparison of the calculated band gaps from the modified 8×8 EFA model and the PL peak positions as measured by 5 K-photoluminescence and the long-wavelength thresholds from FTIR photoresponse measurements. The dashed line is at the 4-μm threshold.

or accuracy of the theory. Overall, the predicted constancy of the gap energies with decreasing SL period is well verified by the experimental data. In the future, we hope to verify the theoretical prediction regarding the improvement in photoresponse and operating temperatures for thin-period SLs and to investigate mixed GaAs-like/InSb-like interfaces as well as the effect of interdiffusion and segregation at interfaces.

4. Conclusions

We used the newly developed 8×8 EFA model that incorporates anisotropic interfacial effects through the Ivchenko-Kaminski-Rössler IF Hamiltonian to design several short-period InAs/GaSb SL structures for the 4-μm detection threshold. The model predicts that is possible to reach the 4-μm for periods as small as several monolayers. The model also predicts that for constant absorption threshold, the SL absorption is independent of the period. However, thinner-period SLs have wider valence band widths and larger intervalence band separations. The former should improve hole effective masses and hole transport while the latter should improve minority electron Auger lifetimes in p-type SLs. These advantages should produce higher photoresponse and detector operating temperatures. The proposed structures were grown by MBE with InSb-like interfaces with SL periods within 0.3% of the nominal designs. The grown samples were characterized by several techniques to ascertain their parameters and quality. The band gap energies were measured by low-temperature photoluminescence and FTIR photoresponse. In qualitative and quantitative agreement with theory, the measured band gaps were found to lie within a narrow band around 4 μm

for SLs in the wide period range between 50.2 to 20.2 Å. Overall, the present work demonstrates the utility of interface design as a tool in the band gap engineering of SLs for IR applications.

Acknowledgments

The work of FS was supported by the Air Force Contract F33615-00-C-5422 at the Materials Lab, AFRL/ML. The authors thank Dr C. Workman and Mr S. Fenstermaker for the lab view program for the shutter sequence and M. S. Fenstermaker for help with the MBE system. B.U.'s work was supported by contract #33. This work was supported by the Air Force Office of Scientific Research (AFOSR/NE) through Lt. Col. Todd Steiner.

References

1. D.L. Smith and C. Mailhiot, *J. Appl. Phys.* **62**, 2545 (1987); *Surface Science* **196**, 683 (1988); *Rev. Mod. Phys.* **62**, 173 (1990).
2. C. Mailhiot and D.L. Smith, *J. Vac. Sci. Technol.* **A7**, 445 (1989).
3. G.J. Brown, F. Szmulowicz, K. Mahalingam, and S. Houston, "Quantum sensing: evolution and revolution from past to future", *Proc. SPIE* **4999**, 457 (2003).
4. J.R. Meyer, C.A. Hoffman, F.J. Bartoli, and L.R. Ram-Mohan, *Appl. Phys. Lett.* **67**, 757 (1995).
5. Q.K. Yang, F. Fuchs, J. Schmitz, and W. Pletschen, *Appl. Phys. Lett.* **81**, 4757 (2002).
6. A. Rogalski, *Prog. Quant. Electr.* **27**, 59 (2003).
7. J. Piotrowski and A. Rogalski, *SPIE* **5359**, 10 (2004).
8. C.H. Grein, W.H. Lau, T.L. Harbert, and M.E. Flatté, *Proc. SPIE*. **4795**, 39 (2002).
9. W.H. Lau and M.E. Flatte, *Appl. Phys. Lett.* **80**, 1683 (2002).
10. F. Szmulowicz, H. Haugan, and G.J. Brown, *Phys. Rev.* **B69**, 155321 (2004).
11. J.N. Schulman and Y.C. Chang, *J. Vac. Sci. Technol.* **B1**, 644 (1983); J.N. Schulman and Y.C. Chang, *Phys. Rev.* **B31**, 2056 (1980); O. Krebs and P. Voisin, *Phys. Rev. Lett.* **77**, 1829 (1996).
12. E.L. Ivchenko, A.Yu. Kaminski, and U. Rössler, *Phys. Rev.* **B54**, 5852 (1996).
13 U. Rössler, and J. Kainz, *Solid State Commun.* **121**, 313 (2002).
14. E.L. Ivchenko, A.A. Toporov, and P. Voisin, *Phys. Sol. State* **40**, 1748 (1998).
15. E.L. Ivchenko and M.O. Nestoklon, *J. Exp. Theor. Phys.* **94**, 644 (2002); *Zh. Exkp. Teor. Fiz.* **121**, 747 (2002).
16. E.L. Ivchenko, A.Yu. Kaminskii, and I.L. Aleiner, *J. Exp. Theor. Phys.* **77**, 609 (1993); E.L. Ivchenko and I.L. Aleiner, *JETP Lett.* **55**, 692 (1992).
17. G. Bastard, *Wave Mechanics Applied to Semiconductor Heterostructures*, Wiley, New York, 1988.
18. G. Bastard, J.A. Brum, and R. Ferreira, "Semiconductor heterostructures, and nanostructures", *Solid State Physics* **44,** 1991.
19. C. Cortez, O. Krebs, and P. Voisin, *Eur. Phy.* **B21**, 241 (2001).
20. L. Vervoort, R. Fereira, and P. Voisin, *Semicond. Sci. and Technol.* **14**, 227 (1999).
21. L. Vervoort, R. Ferreira, and P. Voisin, *Phys. Rev.* **B56**, 12744 (1997).
22. O. Krebs, W. Seidel, J.P. Andre, D. Bertho, C. Jouanin, and P. Voisin, *Semicond. Sci. Technol.* **12**, 938 (1997).
23. P. Ongstad, R. Kaspi, C.E. Moeller, M.L. Tilton, T.M. Gianardi, J.R. Chavez, and G.C. Dente, *J. Appl. Phys.* **89**, 2185 (2001).
24. R. Kaspi, C. Moeller, A. Ongstad, M.L. Tilton, D. Gianardi, G. Dente, and P. Gopaladasu, *Appl. Phys. Lett.* **76**, 409 (2000).
25. E.E. Takhtamirov and V.A. Volkov, *J. Exp. Theor. Phys. Lett.* **71**, 422 (2000); *Pisma Zh. Eksp. Teor. Fiz.* **77**, 612 (2000); E.E. Takhtamirov and V.A. Volkov, *J. Exp. Theor. Phys.* **90**, 1063 (2000), *Zh. Eksp. Teor. Fiz.* **117**, 1221 (2000); E. E. Takhtamirov and V.A. Volkov; *J. Exp. Theor. Phys.* **89**, 1000 (1999), *Zh. Eksp. Teor. Fiz.* **116**, 1843 (1999).
26. B.A. Foreman, *Phys. Rev. Lett.* **81**, 425 (1998); see also *Phys. Rev.* **B54**, 1909 (1996).
27. J.T. Olesberg, W.H. Lau, M.R Flatte, C.Yu, E. Altunkaya, E.M. Shaw, T.C. Hasenberg, and T.F. Boggess, *Phys. Rev.* **B64**, 201301 (2001).
28. K.C. Hall, K. Gundogdu, E. Altunkaya, W.H. Lau, M.E. Flatte, T. Boggess, J.J. Zinck, W.B. Barvos-Carter, and L. Skeith, *Phys. Rev.* **B68**, 115311 (2003).
29. W.H. Lau and M.E. Flatte, *Appl. Phys. Lett.* **80**, 1683 (2002).
30. C.H. Grein, M.E. Flatte, J.T. Olesberg, S.A. Anson, L. Zhang, and T.F. Boggess, *J. Appl. Phys.* **92**, 7311 (2002).
31. H.J. Haugan, F. Szmulowicz , G.J. Brown, K. Mahalingam, *Appl. Phys. Lett.* **84**, 5410 (2004).
32. H.J. Haugan, F. Szmulowicz, G.J. Brown, and K. Mahalingam, *J. Appl. Phys.* **96**, 2580 (2004).
33. Y. Wei, A. Gin, M. Razeghi, and G.J. Brown, *Appl. Phys. Lett.* **80**, 3262 (2000).
34. Y. Wei, A. Gin, M. Razeghi, and G.J. Brown, *Appl. Phys. Lett.* **81**, 3675 (2002).
35. F. Fuchs, E. Ahlswede, U. Weimar, W. Pletschen, J. Schmitz, M. Hartung, B. Jager, J.P. Kotthaus, and F. Szmulowicz, *Appl. Phys. Lett.* **73**, 3760 (1998).
36. H.J. Haugan, L. Grazulis, G.J. Brown, K. Mahalingam, and D.H. Tomich, *J. Cryst. Growth* **261**, 471 (2004).